XIX IMEKO World Congress
Fundamental and Applied Metrology
September 6–11, 2009, Lisbon, Portugal

ESTIMATION OF POSITIVE PARAMETERS IN FORM AND ROUGHNESS ASSESSMENT

Alistair B. Forbes [1] and *João A. Sousa* [2]

[1] National Physical Laboratory, Teddington, UK, alistair.forbes@npl.co.uk
[2] Laboratório Regional de Engenharia Civil, Funchal, Portugal, jasousa@lrec.pt

Abstract – The assessment of the geometry of artefacts in length metrology is concerned with estimating dimension, form and roughness. While all three are positive quantities, the evaluation of form and roughness are problematic, mainly because the values of the parameters to be measured are often of the same order as the measurement uncertainty. Furthermore, random effects associated with a measurement system will in general bias the estimate of parameter. This paper discusses these issues, using a Bayesian approach in which prior distributions are used to ensure parameter estimates are physically meaningful.

Keywords: uncertainty evaluation, form assessment, roughness

1. INTRODUCTION

This paper addresses the problem of measurement of form and roughness in the presence of instrument systematic and random effects. Often, the order of magnitude of the parameter to be assessed, e.g., form error, is similar to that of the uncertainty of the measurement system. In evaluating the uncertainty associated with the fitted parameter, a standard GUM approach [1] is likely to define a coverage interval that includes negative values. Furthermore, the noise in the instrument can introduce significant bias in estimates of the geometrical parameters. For example, random effects associated with the measurement of a perfectly flat table will lead to a measured coordinates that do not lie exactly on a plane. Hence, any standard estimate of the flatness of the table based on the measured coordinates will yield a strictly positive estimate of the flatness. In this paper, we investigate approaches that aim to overcome difficulties of bias and at the same time reflect the positivity constraints associated with the parameters.

In section 2, we describe parameter estimation problems associated with the measurement of surface roughness while in section 3 we examine form error assessment. Both problems can be formulated so that the main computational goal is to estimate two parameters σ^2 and ρ^2 describing the statistical behaviour of the physical systems under study. Our concluding remarks are given in section 4.

2. EXAMPLE: ROUGHNESS

Let ζ_i represent a set of heights of a profile taken at regular intervals along a straight line. The roughness parameter *Rq* associated with the heights is simply defined as the standard deviation ρ of the ζ_i. However, the roughness parameter has to be estimated on the basis of measured estimates z_i of the ζ_i. If the observational model is $z_i \mid \zeta_i \in \mathrm{N}(\zeta_i, \sigma^2)$, that is, given ζ_i, z_i is a draw from a normal distribution with centred at ζ_i with variance σ^2, then the expected value of the variance of the z_i is $\rho^2 + \sigma^2$. Therefore, the variance of the z_i is a biased estimate of *Rq*. If σ is known, and s^2 is the observed variance of the measurements, an unbiased estimate *r* of ρ is given by $r = \left(s^2 - \sigma^2\right)^{1/2}$. However, for very smooth surfaces, there is no guarantee that the observed s will be greater than σ and the estimation method breaks down.

Bayesian approaches [2] enable the positivity constraints on *Rq* to be catered for in a natural way through the use of prior distributions and allow the distribution for *Rq* to be derived. This distribution can then be used in determining optimal limits in assessing whether or not the surface conforms to its roughness specification. One approach is as follows. It is motivated by the fact that the parameters σ^2 and ρ^2 are related to scale parameters representing measures of dispersion. We assign prior distributions for σ^2 and ρ^2 of the form

$$n_0\sigma_0^2\phi \sim \chi^2_{n_0}, \qquad m_0\rho_0^2\psi \sim \chi^2_{m_0}, \tag{1}$$

where $\phi = 1/\sigma^2$ and $\psi = 1/\rho^2$. These distributions encode a degree of belief in the prior estimate ρ_0 for ρ, for example, equivalent to that gained by observing the sum of squares $\rho_0^2 = \sum_{q=1}^{m_0} y_q^2$, where each y_q is sampled from $\mathrm{N}(0, \rho^2)$. In the case of roughness, significant prior knowledge about the instrument accuracy would be reflected

in a large value for n_0; little prior knowledge about the surface roughness would lead to a small value for m_0.

We assume an observational model of the form

$$z_i \in \mathrm{N}(\alpha + \beta x_i, \sigma^2 + \rho^2),$$

where the nuisance parameters α and β account for the linear alignment of the measuring instrument with the surface profile. The aim is to derive a state-of-knowledge distribution for ρ^2 on the basis of the observations. (It is generally more convenient to work with ρ^2 or $\psi = 1/\rho^2$ rather than ρ but the results can be expressed in either form.) The lack of exact knowledge about σ^2 complicates the analysis [3]. If the parameters *a* and *b* specify the least squares best-fit line to the data points (x_i, z_i), $i = 1, \ldots, m$, then the residual sum of squares $F = \sum_{i=1}^{m} (z_i - a - bx_i)^2$ is associated with a chi-squared distribution with $m-2$ degrees of freedom:

$$\frac{F}{\sigma^2 + \rho^2} \in \chi^2_{m-2} \ .$$

This allows us to calculate the probability $p(F \mid \sigma^2, \rho^2)$ of observing *F*, given σ^2 and ρ^2. Bayes' theorem can then be applied to give the posterior distribution for σ^2 and ρ^2 on the basis of the observed value of *F* and the prior distributions:

$$p(\sigma^2, \rho^2 \mid F) \propto p(F \mid \sigma^2, \rho^2) p(\sigma^2) p(\rho^2).$$

The posterior distribution $p(\rho^2 \mid F)$ for ρ^2 is obtained by marginalisation:

$$p(\rho^2 \mid F) = \int_0^\infty p(\sigma^2, \rho^2 \mid F) \mathrm{d}\sigma^2.$$

2.1 Example calculations

We have generated data for the cases *m* = 100, with prior distributions specified as in (3) with $\rho_0 = 0.1$ micrometres, $m_0 = 2$, $n_0 = 100$, and $\sigma_0 = 0.08$, 0.10, 0.12 and 0.15 micrometres. Fig. 1 shows the joint posterior distribution for the case $\rho_0 = \sigma_0 = 0.1$ micrometres while Fig. 2 graphs the posterior distributions $p(\rho^2 \mid F)$. As σ_0 increases, the posterior distributions become more disperse, eventually converging to the prior distribution.

3. FORM ASSESSMENT AND CMM UNCERTAINTY

Coordinate measuring machines (CMMs) are important measurement systems in assessing critical quality characteristics in manufacturing engineering. Form error is one of the features assessed and is a measure of the departure of a manufactured artefact from its ideal shape, specified in terms of standard geometric elements such as planes, spheres, cylinders, etc., or CAD representations such as parametric spline surfaces. The assessment of form error on the basis of measured coordinates will be influenced by the systematic and random effects associated with the CMM as well as the underlying geometry of the artefact being measured. Of particular importance are the parametric errors of the CMM that describe the non-ideal motion of the CMM probe as it moves within the working volume [4].

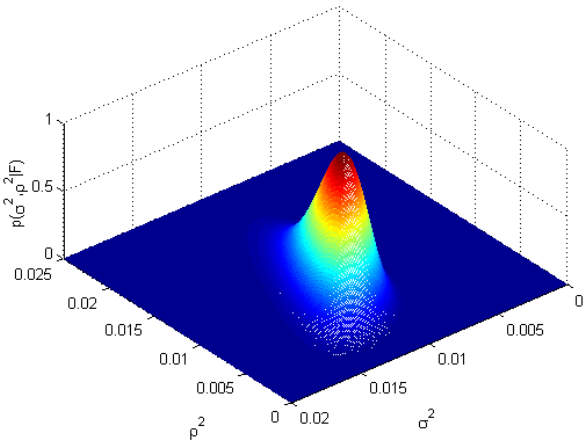

Fig. 1. Posterior distribution $p(\sigma^2, \rho^2 \mid F)$ for the case $\rho_0 = \sigma_0 = 0.1$ micrometres.

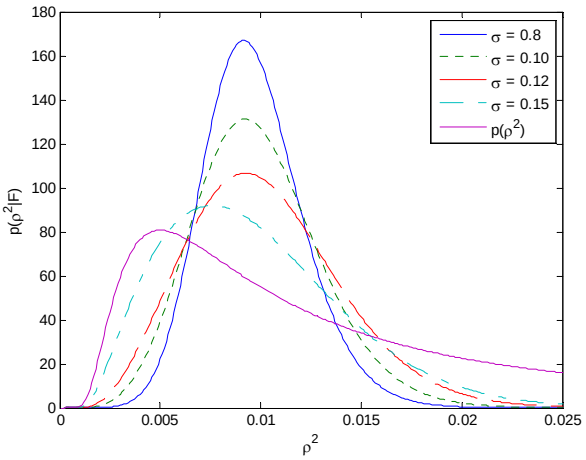

Fig. 2. Posterior distributions $p(\rho^2 \mid F)$ for the cases $\rho_0 = 0.1$ micrometres and $\sigma_0 = 0.08$, 0.10, 0.12 and 0.15 micrometres. The prior distribution $p(\rho^2)$ is also shown.

3.1 Least squares form error assessment

We assume that the CMM outputs measured coordinates $\boldsymbol{x}_i$, $i = 1, \ldots, m_X$, nominally lying on the surface of an artefact whose ideal shape is given parametrically as $(u, v) \mapsto \boldsymbol{s}(u, v, \boldsymbol{b})$. The parameters *u* and *v* determine the position of a point on the surface and the parameters $\boldsymbol{b}$

determine the shape and position of the surface. The least squares best-fit surface can be found [4] by minimising

$$\sum_{i=1}^{m_X} d^2(\boldsymbol{x}_i, \boldsymbol{b}), \qquad d(\mathbf{x}_i, \mathbf{b}) = (\mathbf{x}_i - \mathbf{s}(u_i^*, v_i^*, \mathbf{b}))^{\mathrm{T}} \mathbf{n}_i, \quad (4)$$

where u_i^* and v_i^* specify the point $\boldsymbol{s}_i^* = \boldsymbol{s}(u_i^*, v_i^*, \boldsymbol{b})$ on the surface closest to $\boldsymbol{x}_i$ and $\boldsymbol{n}_i$ is the normal vector at $\boldsymbol{s}_i^*$. The form error is estimated by $f_E = \max_i d_i - \min_i d_i$, where the d_i are the residual errors at the solution. Also of interest is the standard deviation *s* of the residuals.

3.2 Measurement model

We assume that the CMM measurement model is of the form

$$\mathbf{x}_i = \mathbf{x}_i^* + \mathbf{p}(\mathbf{x}_i, \mathbf{a}) + \mathbf{e}_i,$$

where $\boldsymbol{x}_i$ is the reported measured coordinates, $\boldsymbol{x}_i^*$ the true coordinates, $\boldsymbol{p}(\boldsymbol{x}_i, \boldsymbol{a})$ the systematic parametric error at $\boldsymbol{x}_i$ depending on parameters $\boldsymbol{a}$, and $\boldsymbol{e}_i$ is a random effect. We assume that the CMM has been calibrated so that estimates of $\boldsymbol{a}$ and its variance matrix $V_{\boldsymbol{a}} = \sigma^2 V_{\boldsymbol{a},0}$ are available. The matrix $V_{\boldsymbol{a},0}$ is fixed and the parameter σ^2 is a scaling factor for which there is prior information encoded in a distribution $p(\sigma^2)$. This prior information can be provided in a calibration of the CMM's parametric errors. The random effects are assumed to be independently distributed with standard deviation τ_0.

3.3 Form error model

We assume that the departure from ideal geometry is modelled as

$$\mathbf{x}_i^* = \mathbf{s}_i^* + f_i \mathbf{n}_i,$$

where f_i is the departure from nominal geometry, specified normal to the surface. We assume that the vector $\boldsymbol{f} = (f_1, \ldots, f_{m_X})^{\mathrm{T}}$ of departures from ideal geometry is drawn from a multinormal distribution with mean zero and variance matrix $V_{\boldsymbol{f}} = \rho^2 V_{\boldsymbol{f},0}$, where the matrix $V_{\mathbf{f},0}$ is fixed and the parameter ρ^2 is a scaling factor with associated prior distribution $p(\rho^2)$. For most engineering surfaces, the departure from ideal geometry varies smoothly across the surface so that the departure from ideal geometry will be similar for points close to each other. This correlation effect can be encoded in the matrix $V_{\boldsymbol{f},0}$. For example, we can set

$$V_{\mathbf{f},0}(i,q) = \exp\left\{-\frac{1}{2}\left(\mathbf{s}_i^* - \mathbf{s}_q^*\right)^{\mathrm{T}} M \left(\mathbf{s}_i^* - \mathbf{s}_q^*\right) - \frac{\kappa^2}{2}\right\},$$

so that the correlation decays exponentially with the square of the distance between points. The 3×3 matrix *M* allows for the correlation behaviour to be different in different directions. The term κ allows for some variation at small scales due to roughness.

Putting the measurement and form error models together we have

$$\boldsymbol{x}_i = \boldsymbol{s}_i^* + f_i \boldsymbol{n}_i + \boldsymbol{p}(\boldsymbol{x}_i, \boldsymbol{a}) + \boldsymbol{e}_i.$$

From the measurement data $\boldsymbol{x}_i$, we calculate a least squares best fit surface to the data, returning the residual vector $\boldsymbol{d} = (d_1, \ldots, d_{m_X})^{\mathrm{T}}$. The main goal is to be able to determine an improved estimate of ρ^2 (and potentially σ^2) on the basis of the additional information provided by the observed residual vector ***d***.

3.4 Effect of CMM uncertainty on form error assessment for ideal geometries

Suppose $\boldsymbol{s}_i^*$ lies exactly on a surface with ideal geometry,

$$\boldsymbol{x}_i = \boldsymbol{s}_i^* + \boldsymbol{p}(\boldsymbol{x}_i, \boldsymbol{a}) + \boldsymbol{e}_i$$

represents CMM measurements and ***d*** the residual error vector. If *J* is the Jacobian matrix associated with the best-fit surface and $J = \begin{bmatrix} Q_1 & Q_2 \end{bmatrix} \begin{bmatrix} R_1 \\ 0 \end{bmatrix} = Q_1 R_1$ is its QR factorisation, then to first order $\mathbf{d} = Q_2 Q_2^{\mathrm{T}} \mathbf{h}$, where $\boldsymbol{h}$ is the m_X-vector storing $\boldsymbol{n}_i^{\mathrm{T}} (\boldsymbol{p}(\boldsymbol{x}_i, \boldsymbol{a}) + \boldsymbol{e}_i)$. Uncertainties associated with $\boldsymbol{a}$ and the random effects associated with the CMM measurements are easily propagated through to ***d***, so that the variance matrix $V_{\boldsymbol{d}} = V_{\boldsymbol{d}}(\sigma^2)$ can be calculated.

To illustrate this approach, we consider a model of a CMM with scale and squareness errors [5] so that

$$\boldsymbol{p}(\boldsymbol{x}, \boldsymbol{a}) = \begin{bmatrix} a_{xx} & a_{xy} & a_{xz} \\ 0 & a_{yy} & a_{yz} \\ 0 & 0 & a_{zz} \end{bmatrix} \boldsymbol{x}.$$

The diagonal elements represent the scale errors along the three axes while the non-zero off-diagonal elements are the squareness errors. We assume there are 12 measured points on a cylinder of radius 50 mm, four points on three circles 25 mm apart. We assume that $\tau_0 = 0.001$ mm and that

$$\boldsymbol{a} = (a_{xx}, a_{yy}, a_{zz,} a_{xy}, a_{xz}, a_{yz})^{\mathrm{T}}$$

is associated with $\mathrm{N}(0, \sigma^2 I)$ with $\sigma = 5 \times 10^{-5}$. For this statistical model, the standard uncertainties associated with the point coordinates are of the order of 0.003 mm. From the statistical model so defined, the distribution $\mathrm{N}(0, V_{\boldsymbol{d}}(\sigma^2))$ for the residual vector can be calculated. We have generated 10,000 Monte Carlo samples $\boldsymbol{d}_q$ from this distribution and calculated the associated form errors $f_{E,q}$ and standard deviations s_q. Histograms of the calculated $f_{E,q}$ and s_q are shown in Figs. 3 and 4. The calculations indicate that the expected estimate of the form error, derived

from the residual vector, due to CMM uncertainty alone is almost 0.005 mm.

3.5 Posterior estimate of ρ^2

The approach above can be extended to incorporate the form error model, with $\boldsymbol{h}$ now defined to be the m_X vector storing $f_i + \boldsymbol{n}_i^{\mathrm{T}}(\boldsymbol{p}(\boldsymbol{x}_i, \boldsymbol{a}) + \boldsymbol{e}_i)$. The uncertainty information is propagated through to $\boldsymbol{d}$ and the associated variance matrix $V_{\boldsymbol{d}} = V_{\boldsymbol{d}}(\sigma^2, \rho^2)$ now depends also on ρ^2. This matrix will in fact be rank deficient. However, the projected residual vector $\hat{\boldsymbol{d}} = Q_2^{\mathrm{T}}\boldsymbol{d} = Q_2^T\boldsymbol{h}$ has associated variance matrix $Q_2^{\mathrm{T}}V_{\boldsymbol{d}}Q_2$ which is full rank and allows us to calculate the probability distribution

$$p(\hat{\boldsymbol{d}} \mid \sigma^2, \rho^2) \propto \left|Q_2^T V_{\boldsymbol{d}} Q_2\right|^{-1/2} \exp\left\{-\frac{1}{2}\hat{\boldsymbol{d}}\left(Q_2^T V_{\boldsymbol{d}} Q_2\right)^{-1}\hat{\boldsymbol{d}}\right\},$$

for observing $\hat{\boldsymbol{d}}$, given σ^2 and ρ^2. (The dependence on σ^2 and ρ^2 is through $V_{\boldsymbol{d}} = V_{\boldsymbol{d}}(\sigma^2, \rho^2)$.) An application of Bayes' theorem enables us to calculate the posterior distribution $p(\sigma^2, \rho^2 \mid \hat{\boldsymbol{d}})$.

3.6 Example calculations

Fig. 5 shows the posterior distribution for ρ^2 having observed the projected residuals $\hat{\boldsymbol{d}}$ associated with measuring a cylinder using a CMM with uncertainties associated with scale and squareness errors and three measurement strategies involving 12, 25 and 75 data points.

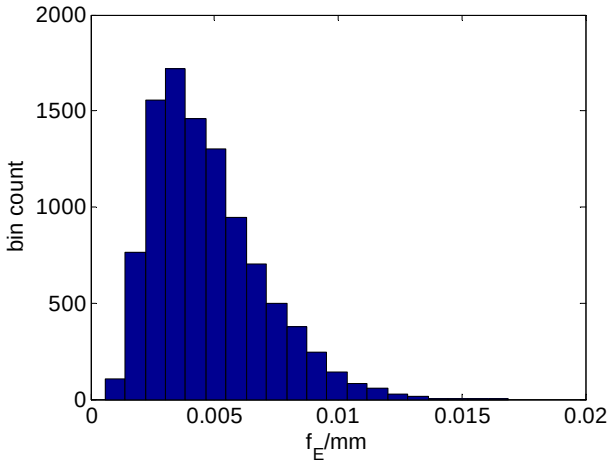

Fig. 3. Histogram of $f_{E,q}$.

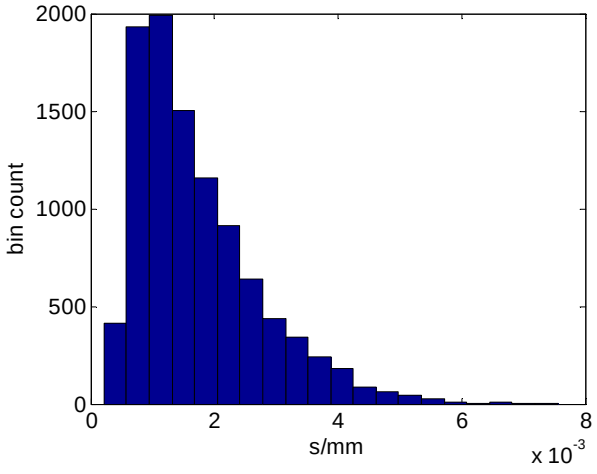

Fig. 4. Histogram of s_q.

The prior distributions for σ^2 and ρ^2 are of the same form as (1), with $\sigma_0 = 1$ and n_0 = 1000, signifying that the CMM is well characterised, and $\rho_0 = 0.005\,\mathrm{mm}$ and $m_0 = 5$, signifying little prior information about the surface form error. As the number of data points increases the posterior distribution becomes more peaked. For a small number of data points, the uncertainty associated with ρ^2 is dominated by small sample effects (i.e., trying to estimate a standard deviation from a small sample). For a large number of points, the influence of CMM uncertainty becomes stronger. For the larger data set, the effect of correlation in the form error also becomes more important.

The analysis is straightforward to implement in that it only requires linear algebra and simple quadrature. However, it does provide uncertainty information about form error that takes into account the CMM random and systematic effects, surface geometry and likely form error. In particular, the interaction between CMM parametric errors and form error is properly taken into account so that, for example, the uncertainty associated with a global scale parameter (that contributes to the uncertainties associated with all the coordinates) will not introduce form error where none exists.

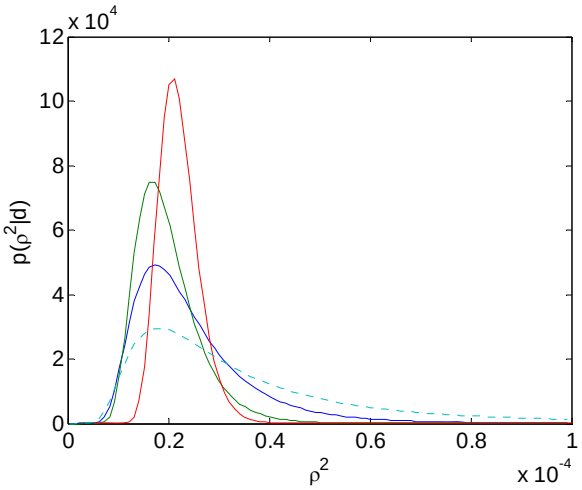

Fig. 5. Prior (dotted) and posterior distributions for ρ^2 for 12, 25 and 75 data points. As the number of data points increases, the peaks for the posterior distributions become sharper.

3.7 Separating form and CMM error

The analysis so far has examined the combined effect of CMM uncertainty and form error on the projected residuals associated with a least squares best fit of a surface to data. However, a more direct examination of the form error or CMM parametric errors from the residuals errors is often sought. For example, the measurement of a calibrated ring gauge with a very low form error will tell us something about the CMM parametric errors. Given σ^2 and ρ^2 and observed projected residuals $\hat{\boldsymbol{d}}$, posterior estimates $\hat{\boldsymbol{a}}$ and $\hat{\boldsymbol{f}}$ of the machine error parameters and form error can be found by solving a linear least squares system

$$\begin{bmatrix} C_{11} & C_{12} \\ C_{21} & 0 \\ 0 & C_{32} \end{bmatrix} \begin{bmatrix} \boldsymbol{a} \\ \boldsymbol{f} \end{bmatrix} = \begin{bmatrix} \hat{\boldsymbol{d}} \\ 0 \\ 0 \end{bmatrix},$$

where the first set of equations describes the machine and form error contribution to the observed projected residuals, and the second and third sets represent the prior information about the machine and form errors.

Figs. 6 and 7 show the results of an application of this approach, this time concerning the measurement of 15 points on a sphere, 5 points on three parallel circles. The graphs show how each residual can be decomposed as the sum of form error, machine error and random effects. The results in Fig. 6 concern the measurement of an artefact with significant form error. The observed residuals are attributed to the form error. Fig. 7 relates to the measurement of a calibrated sphere that has a form error of no more than 0.000 5 mm. In this case, the residuals are explained mainly in terms of machine errors $\boldsymbol{a}$. Examining the posterior estimate of the variance matrix associated with $\boldsymbol{a}$ shows that the standard uncertainties associated with the scale and squareness parameters are $10^{-5} \times (3.1, 3.1, 3.2, 1.9, 1.7, 1.7)$ and can compared with the prior values of 5×10^{-5}. The standard uncertainties in the squareness parameters are reduced more than the scale parameters. This is because a global increase in the scale will not affect the form error. However, posterior to the data, the scale error parameter estimates are now correlated; different scale errors along each axis are now very unlikely.

The analysis can be extended to include the case where the parameters σ^2 and ρ^2 are no longer regarded as fixed. The fact that the parameters $\boldsymbol{a}$ and $\boldsymbol{f}$ appear linearly in the model means that they can be eliminated analytically in a marginalisation process in order to evaluate $p(\sigma^2, \rho^2 \mid \hat{\boldsymbol{d}})$. Perhaps more interesting is the use of reversal strategies that are able to give a much more concrete separation of the effects of form and machine error. These strategies are currently under study.

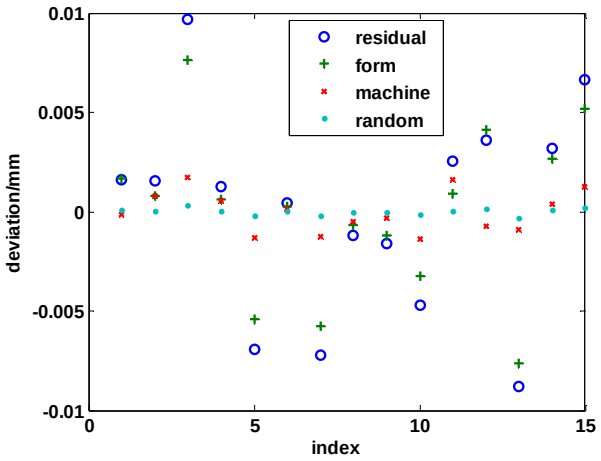

Fig. 6. Explanation of the observed residuals in terms of form error, CMM machine errors (scale and squareness) and random effects.

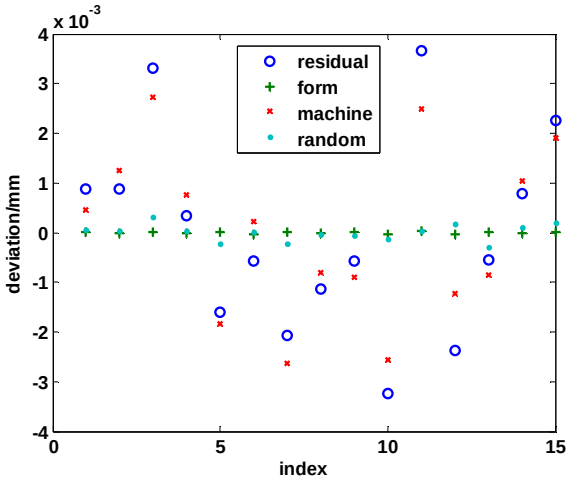

Fig. 7. As Fig. 6, but for the measurement of a calibrated sphere with small form error.

4. CONCLUSIONS

The GUM uncertainty framework can run into difficulties in limit-of-detection problems since the

construction of coverage intervals based on measured values and associated expanded uncertainties will often lead to the inclusion of negative values in the category of "values that could reasonably be attributed to the measurand". Bayesian methods, on the other hand, are capable of handling limit-of-detection problems, as illustrated in the two case studies above. Having more reliable estimates of the surface roughness or form error will lead to smaller decision costs associated with conformance assessment [3, 6].

ACKNOWLEDGMENTS

The work described in this paper was supported by the National Measurement System Directorate of the UK Department for Innovation, Universities and Skills as part of the NMS Software Support for Metrology programme. This work was also supported by the British Council and FCT (Portugal) under the Grices protocol joint programme. We thank Dr Ian Smith and Dr Hoang D Minh, NPL, for comments on earlier drafts of this paper.

REFERENCES

[1] BIPM, IEC, IFCC, ISO, IUPAC, IUPAP and OIML "*Guide to the Expression of Uncertainty in Measurement*" 2nd edn (Geneva: International Organization for Standardization), 1995.

[2] A. Gelman, J. B. Carlin, H. S. Stern and D. B. Rubin, *Bayesian Data Analysis*, Chapman & Hall/CRC, Boca Raton, 2004.

[3] J. A. Sousa and A. B. Forbes, "Optimal decision rules and limits of detection", *VIII AMCTM International Conference*, Pavese et al., eds., pp. 319-325, 2009.

[4] G. Zhang, *et al*., "A displacement method for machine geometry calibration", *Ann. CIRP*, vol. 37, pp. 515-518, 1988.

[5] A. B. Forbes, "Surface fitting taking into account uncertainty structure in coordinate data", *Meas. Sci. Tech.*, vol. 17, pp. 553-558, 2006.

[6] A. B. Forbes, "Measurement uncertainty and optimised conformance assessment", *Measurement*, vol. 39, pp. 808-814, 2006.